Journal of Materials Chemistry

Dynamic Article Links

Cite this: J. Mater. Chem., 2012, 22, 7863

www.rsc.org/materials

PAPER

Chemical assisted formation of secondary structures towards high efficiency solar cells based on ordered TiO_2 nanotube arrays†

Liang Tao,[a] Yan Xiong,[b] Hong Liu*[a] and Wenzhong Shen*[ab]

Received 1st January 2012, Accepted 21st February 2012
DOI: 10.1039/c2jm00005a

Amongst all types of photoanodes in sensitized solar cells, nanotube arrays (NTs) have become a suitable choice that can balance the dye absorption, electron transport, and effective thickness. However, the maximum performance they have shown now is still not comparable with porous films. In this work, we have established a simple yet effective method towards high performance solar cell based on NTs. Significantly increased carrier generation by better dye absorption can be realized by the particle-like secondary structures grown on TiO_2 tubes. Nevertheless, this effect was often followed by a sacrifice of the electron transport properties of the NTs, which may greatly weaken the total net increase of efficiency by the secondary structures. With a subsequent $TiCl_4$ treatment and slightly modulated outer conditions (anodic voltage and stirring rate), we are able to adequately resolve this paradox. The short circuit current can be raised to over 110% higher, while the fill factor and open circuit voltage remain unharmed. As a result, an efficiency of 4.35% can be achieved in the back-side illuminated dye-sensitized solar cells, which is ~114% higher than the basic efficiency of the plain cell. The formation of the secondary structures can be explained by the reversible dissolution-reprecipitation of TiO_2 with the reaction-diffusion process of F^- and other fluoride species during the treatment.

1. Introduction

As a broadband semiconductor, TiO_2 has attracted a great deal of attention due to its excellent stability, photocatalytic ability and feasibility for various nanostructure fabrications.[1–3] Since originally reported by O'Regan and Grätzel,[4] the application of TiO_2 in dye-sensitized solar cells (DSSCs) are currently applied in widespread scientific and technological regions. Up to now, the most excellent nanoporous (NP) film based DSSC with single dye can reach nearly 13% by using the YD2-o-C8 dye and a high potential reduction/oxidation pair (cobalt (II/III)-based redox electrolyte) developed by the Grätzel group.[5] The large surface area of the NP film enables better absorption of the sensitizers, therefore enables more efficient light harvesting and carrier generation. Nevertheless, electron transport is a limiting factor on the performance of these NP crystalline electrodes due to the interface effects between two crystalline nanoparticles, which leads to enhanced scattering of free electrons and thus reduces the electron mobility.[6] Furthermore, the irregular organization of particles inside the NP films would also reduce the real effective absorption surface area for the sensitizers due to a possible block on the path into the depth of the porous layer.[7–10]

In recent years, a great many efforts have been paid to explore better performed DSSCs. One of the well known methods was to apply mesoporous/P25 film using a sol-gel approach based on block copolymers, which has achieved a fairly high efficiency.[11] Another important approach is to research new photoanodes in place of the single porous TiO_2 films in order to further enhance the performance of the DSSCs. In a greater degree of variation, the ordered nanotube arrays (NTs) have been another recent focus which can hopefully offer higher carrier transport ability and less blocking effect of the sensitizer absorption than the NP films. It has been pointed out that the NTs-based DSSCs have higher charge-collection efficiencies than those of the NP-based ones by the Frank group.[8] The work by the Schmuki group has achieved the first meaningful efficiency in DSSCs based on ordered TiO_2 NTs under AM 1.5 illumination.[12] About 2–3% efficiency of DSSCs based on the pure TiO_2 NTs were later obtained.[13–15] To achieve better performance, further studies on the TiO_2 NTs-based DSSCs have been made *via* various approaches, mainly from morphology control and chemical implantation. It was reported that for the same diameter the optimum tube length was around 20 μm,[9] meanwhile for the same thickness of nanotube, a smaller diameter helps to achieve

[a]*Laboratory of Condensed Matter Spectroscopy and Opto-Electronic Physics, and Key Laboratory of Artificial Structures and Quantum Control (Ministry of Education), Department of Physics, Shanghai Jiao Tong University, 800 Dong Chuan Road, Shanghai, 200240, People's Republic of China. E-mail: liuhong@sjtu.edu.cn; Fax: +86 (0)21 54743243; Tel: +86 (0)21 54743243*

[b]*Institute of Solar Energy, Department of Physics, Shanghai Jiao Tong University, 800 Dong Chuan Road, Shanghai, 200240, People's Republic of China. E-mail: wzshen@sjtu.edu.cn; Fax: +86 (0)21 54747552; Tel: +86 (0)21 54747552*

† Electronic supplementary information (ESI) available: Further details. See DOI: 10.1039/c2jm00005a

higher efficiency.[10,13] More recent research has indicated that for the same efficiency, the necessary thickness of photoanodes based on oriented nanostructures is much less than those based on NP films.[15–18] This is especially helpful for flexible or transparent cells.

Nevertheless, the normal efficiency of DSSCs based on pure TiO_2 NTs is still lower than that based on nanocrystalline TiO_2 porous films,[5] which is usually made by sintering a paste consisting of colloidal oxide particles with sizes in the 10–30 nm range. In order to resolve this issue, different approaches have been studied in recent years. One factor has been contributed to the reduction of electron transport in the tube arrays. This problem may have come from different reasons, for example, the trapping effect of oxygen defects in the TiO_x ($x \leq 2$) bulk, which often appears after the anodiztion due to incomplete oxidation.[19] With oxygen plasma treatments assisted with chemical treatment, TiO_2 NTs-based DSSCs have exhibited an overall efficiency of 7.37%.[20] Another important factor is the relatively smaller total surface area of the tubes with a smooth surface compared to the NP ones, which can be hopefully overcome by modifications on the surfaces. One usual surface modification is creating secondary structures by applying the chemical treatments through etching or precipitation.[18,21,22] However, the chemical treatments may induce problems such as irregular morphological change at the tube surface and damages in the tube bulk, which negatively influences the electron transport and thus reduce the total efficiency.[23,24] Hence to a certain degree a paradox lies between the improvement of the two factors.

In this work, a simple and efficient fabrication method to modify and improve the TiO_2 NTs has been demonstrated, which can create a balance between the carrier transport and the dye absorption. Extradimensional fine structures, *i.e.*, additional islands on the tube walls were developed after being soaked in HF solutions and then annealed to 500 °C. Such a fine structure was proved to induce a significant increase of short circuit current and efficiency ($\Delta\eta/\eta_0 > 35\%$) from the plain DSSC (back-side illuminated model, see Fig. 1 in the ESI†). The back-side illuminated model has a low basic efficiency but offers identical initial experimental conditions to study the method.

Moreover, the impedance of the sensitizer installation and electron transport brought by those secondary structures could be compensated by $TiCl_4$ treatment and application of oscillating voltages and mechanical stirring. Combining those methods, an increase of ~114% from the basic efficiency of plain DSSCs has been realized. The spectroscopic analysis on the formation of those islands described the recombination process at the wall surface by the reversible chemical etching process of TiO_2 with F^- anions. Generally speaking, the presented method introduced an effective approach to raise the cell efficiency with greatly enhanced short circuit current from both the dye installation and the carrier transport, which is able to play a significant role in the advancement of DSSCs and other devices relying on similar materials.

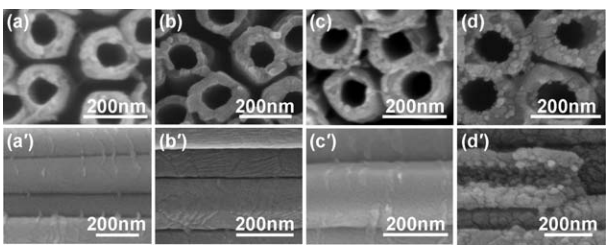

Fig. 1 FE-SEM images of oriented TiO_2 tube arrays grown from a 250 nm thick Ti sheet by 10 min, (a), (b) without and (c), (d) with HF treatment (soaked in a 0.1% HF aqueous solution for 30 min at room temperature within airtight bottles). (a), (c) show the top view of the as-prepared TiO_2 NTs before annealing; (b), (d) show the top view of annealed TiO_2 NTs. (a′)–(d′) show the lateral view of corresponding TiO_2 NTs under the same conditions.

2. Experimental

2.1 Fabrication of TiO_2 nanotube arrays

The Ti sheets (0.25 mm thick, 99.7% purity, Sigma-Aldrich Co. Ltd., USA) were cleaned with methanol, ethyl alcohol, acetone and isopropyl alcohol with ultrasonication in sequence to remove any impurities. Highly ordered TiO_2 NTs were prepared by a second anodization of the Ti sheet in a two-electrode cell. The first anodization was performed at 180 V at 5 °C for 60 min in a solution of 0.09 M NH_4F and 1.0 wt% of H_2O in ethylene glycol (E.G.). The second anodization was performed at 180 V/180 ± 5 V at 5 °C for 10 min in the same solution. The anodized Ti sheet was rinsed with deionized water and ethanol, followed by annealing in air at 500 °C for 1 h at a heating rate of 10 °C per min. Then the TiO_2 film was carefully cleaned in deionized water with ultrasonication. The TiO_2 NT films used in the following experiments have a standard inner and outer diameter of about 100 nm and 200 nm, respectively.

2.2 Growth and modification of TiO_2 NTs with secondary structure

To develop the secondary structures on the nanotubes, the TiO_2 film was first soaked in a 0.1% HF solution (volume ratio of saturated HF and H_2O is 1 : 1000) for 30 min at room temperature within airtight bottles. After airing, the HF treated TiO_2 NT film was annealed at 500 °C for 1 h. In the $TiCl_4$ treatment, the sample was first soaked in a 0.2 M $TiCl_4$ solution for 60 min at room temperature within airtight bottles. Then it was annealed under the same conditions as the HF treatment. The digital pictures of TiO_2 NT films at different stages can be found in Fig. 2 in the ESI.†

2.3 Fabrication of DSSCs

The TiO_2 NT films with or without HF/$TiCl_4$ treatment were sintered in air for 1 h at 500 °C (each with an area of 0.25 cm^2), then immersed in 0.5 mM N719 dye (Ruthenium 535-bisTBA) solution in ethanol for 12 h. These films were used as the photoanodes and mounted together with a counter electrode with platinum black (prepared by coating FTO glass with a 4 mM H_2PtCl_6 solution in ethanol and then heating in air at 200 °C for 60 min) to form back-side illuminated cells. The liquid electrolyte was injected into the cells by a syringe, which consisted of 0.1 M iodine (I_2), 0.1 M lithium iodide (LiI), 0.6 M tetra-butylammonium iodide and 0.5 M 4-*tert*-butyl pyridine in acetonitrile (CH_3CN, 99.9%).

2.4 Characterization of the materials and devices

The surface morphologies of the samples were characterized by a field emission scanning electron microscope (FE-SEM, JEOL JSM). The elemental analysis was performed by the energy dispersive X-ray (EDX) during the FE-SEM observation. A transmission electron microscope (TEM, JEM-2100F, JEOL USA Inc.) was employed to investigate the detailed structural information of the TiO_2 NT materials. Detailed microstructures were investigated by the selected area electron diffraction (SAED) during the high-resolution (HR)-TEM measurements. The microstructures of the samples were characterized by X-ray diffraction (XRD, D/max-2200/PC) with high intensity Cu-Kα radiation ($\lambda = 1.5406$ Å). The Raman spectra were taken at room temperature on a Jobin Yvon LabRAM HR 800UV micro-Raman system with the excitation of a He-Cd laser (325.0 nm). The photocurrent density-photovoltage (J-V) characteristics of the DSSCs with an active area of 0.25 cm^2 were measured under AM 1.5 (100 mW cm^{-2}) illumination provided by a solar simulator (Oriel Sol 2A) with a Keithley 2400 source meter. More data can be found in Table 1 in the ESI.†

3. Result and discussion

3.1 Development of the secondary structure on the TiO_2 NTs

In order to study more systematically, experiments were firstly carried out with only HF enrollment. The TiO_2 NTs were fabricated with the standard procedure that has been usually applied for better indentities.[25,26] The anodization voltage was chosen to be 180 V and the temperature was 5 °C so that the tubes could be growth in a relatively fast rate with good quality. A second anodization for 10 min was carried out to form more ordered tube arrays in a controlled short length to meet the requirement of the DSSCs. The so-fabricated NTs in those different stages are shown in Fig. 1(a), (a′), (b) and (b′). They all had quite uniform sizes, *i.e.*, the inner diameter, outer diameter and thickness of 110 nm, 215 nm and 21 μm, respectively. The tubes have smooth inner and outer surfaces and straight shape before annealing, and contain some small corrugation on the surface after annealing.

However, after the HF treatment, a series of secondary structures appeared at the surface of the TiO_2 tubes compared to the tubes without the preliminary HF treatment, as shown in Fig. 1(c), (c′), (d) and (d′). In detail, numerous multidimensional fine structures emerged around the surface of NTs after the tubes were annealed, while few multidimensional fine structures appeared before the tubes were annealed. It is worth mentioning that the inner/outer diameter of tubes remained at the original size while the surface became rougher. It can also be seen from Fig. 1(d′) that these particles were also grown at the inside surface of the tubes.

3.2 Structural analysis of TiO_2 NT films with HF treatment

Beside the surface morphological change shown in Fig. 1, changes can also take place in the inner morphology and microstructures. Therefore the TEM measurement was carried out together with SAED patterns. Fig. 2(a)–(d) show the magnified TEM images of the TiO_2 NTs with/without HF treatment. These results clearly show that after the HF treatment and annealing, the inner surface of the tubes also became much rougher than the one without HF treatment after annealing, and the diameter of the nanotubes was hardly affected. Compared to Fig. 1(c′) and (d′), similar secondary structures to the outer surface were formed with HF treatment and annealing, with an average size ranging from 12 to 25 nm. It can also be more clearly observed from Fig. 2 that the development of those secondary structures mainly happened after the sample was already taken out of the HF solution, and during the annealing. The corresponding SAED pattern shown in Fig. 2(e) and (f) confirms the changing from amorphous phase to crystalline phase and the highly crystalline nature of anatase TiO_2. The SAED data has indicated that the TiO_2 was polycrystalized and more or less randomly oriented. The crystalline structures could also be identified in the HR-TEM images shown in Fig. 2(g) and (h).

Though the SAED and the HR-TEM images have shown crystallinity of the so-fabricated TiO_2 NTs, they have only shown the localized information. For more macroscopic information, the XRD and the Raman spectroscopy are necessary. Fig. 2(i) shows the corresponding XRD pattern of the HF-treated TiO_2 tube arrays. All diffraction peaks of the as-prepared tubes after annealing at 500 °C exhibit good agreement with anatase reference data,[27] indicating that the HF-treated TiO_2 NTs are well crystalline after the widely-used annealing method. Fig. 2(j) shows the room temperature Raman spectrum recorded between 100 and 700 cm^{-1}. It exhibits five distinct and strong peaks at about 143.9, 195, 399.3, 518.6 and 637.8 cm^{-1} in the Raman

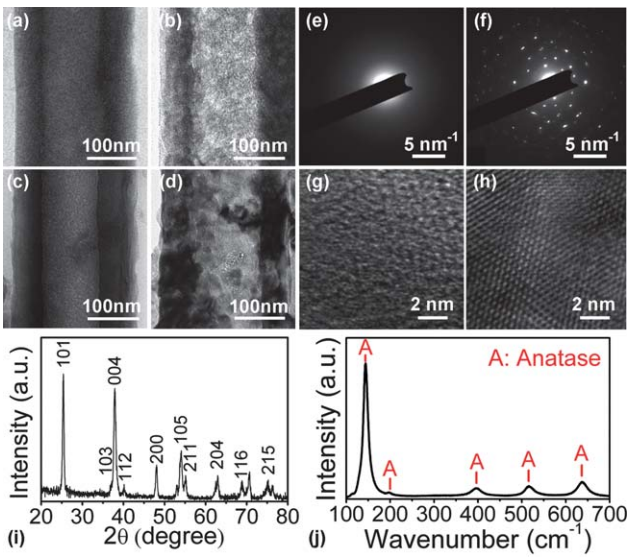

Fig. 2 Analysis of the TiO_2 tubes with HF treatment. (a)–(d) TEM images of the TiO_2 NTs: (a) without HF treatment, before annealing; (b) without HF treatment, after annealing; (c) with HF treatment, before annealing; and (d) with HF treatment, after annealing. (e), (f) SAED pattern of the TiO_2 NTs with HF treatment: (e) before annealing; and (f) after annealing. (g), (h) HR-TEM images of the TiO_2 NTs with HF treatment: (g) before annealing; and (h) after annealing. (i) XRD pattern of the TiO_2 tubes with HF treatment, sintered in air for 1 h at 500 °C at a heating rate of 10 °C per min. (j) Room temperature Raman spectra of the anodized tubes with HF treatment, sintered under the same conditions.

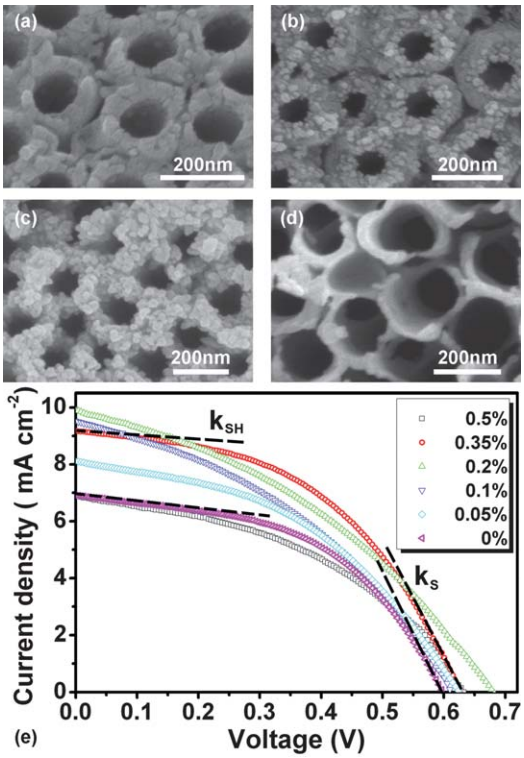

Fig. 3 TiO_2 tube arrays after annealing at 500 °C, pre-treated with HF in different concentrations: (a) 0.05%, (b) 0.2%, (c) 0.35%, (d) 0.5% HF treatment. (e) J-V characteristics of dye-sensitized solar cells (using N719) with the TiO2 NTs treated by various HF aqueous solution concentrations, at a constant illumination of 100 mW cm^{-2}. The dashed lines marked by k_{SH} and k_S indicate the slopes near J_{SC} and V_{OC}, which are related to the reciprocals of shunt resistance and series resistance, respectively.

spectrum of the annealed TiO_2 tube arrays, revealing that the lattice atoms are aligned in anatase phase, which agrees well with the observation for TiO_2 thin films by Fujiki and other groups.[28–30] Those results above indicated that the so-fabricated TiO_2 NTs were ready to be used in the DSSCs.

3.3 Photovoltaic performance of DSSCs based on TiO_2 NTs treated by HF aqueous solution in various concentrations

As demonstrated in sec. 3.2, secondary structures on the TiO_2 surfaces were formed with 0.1% HF treatment and have shown good crystallinity after annealing. It would be interesting to investigate the evolution of this phenomenon *versus* different conditions. Hence similar experiments have been carried out with a series of HF conditions and the results are shown in Fig. 3(a)–(d). When the HF concentration increased, first the density of particles on the surface increased, then reached a maximum. When the HF concentration continued to rise up, the tube surface became smooth again. Combining the results in Fig. 1(a) and (c), apparently these kind of island-particles reach the highest density with an intermediate HF concentration of about 0.35%.

Consequently, this multidimensional fine structure gave rise to a corresponding improvement of DSSCs based on those TiO_2 NTs. The as-fabricated samples were mounted with a counter electrode (Pt black) to form a back-side illuminated dye-sensitized solar cell (using N719 as the sensitizer). Though the back-side illuminating form of the DSSC would suppress the total conversion efficiency, it would not harm the effect of secondary structures. Fig. 3(e) presents the J-V characteristics of the DSSCs. For a solar cell without HF processing, the measurement yielded the efficiency of 2.03% (curve 0% in Fig. 3(e)), with an open circuit voltage (V_{OC}) of 0.60 V, a short circuit current density (J_{SC}) of 6.90 mA cm^{-2}, and a fill factor (FF) of 0.49. When the TiO_2 NTs processed by various concentration of fluoride were applied into DSSCs, the cell performance was increased significantly (see curve 0.05%, 0.1%, 0.2%, 0.35% and 0.5% in Fig. 3(e)), as the HF concentration increases from 0%. The best efficiency was 2.75% at the 0.35% HF concentration, with V_{OC} = 0.62 V, J_{SC} = 9.16 mA cm^{-2}, and FF = 0.49. Compared to its non-HF treated counterpart, it represents an increase of 32.75% of the short circuit current and 35.47% of the efficiency. These improvements can be contributed to the increase of dye absorption due to higher effective surface-to-volume ratio by those secondary crystal structures. However, after the development of the secondary structures on the tubes, the contact between those particles and the tube surfaces is sometimes not good, and too many particles might stack together and too much of a steep surface roughness can sometimes block the penetration of the dye molecule to the depth of the tubes. Both these factors can both reduce the improvement of the cell efficiency.[31,32]

Furthermore, as widely known in the solar cell characterization, the slope of the J-V curve at different positions can represent the resistances inside the solar cell, *i.e* the slopes near the V_{OC} (k_S) and J_{SC} (k_{SH}) are proportional to the reciprocals of the

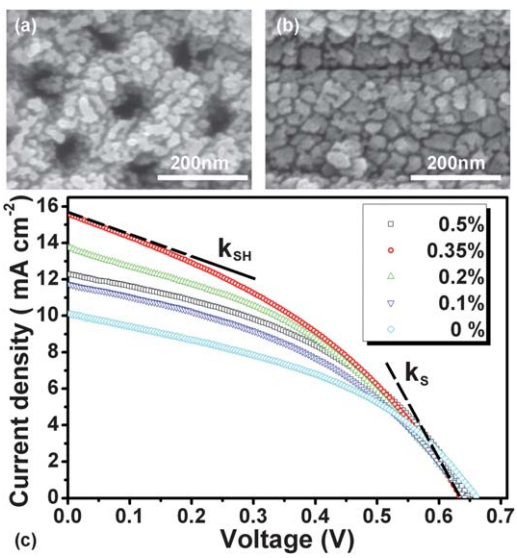

Fig. 4 TiO_2 NTs with 0.35% HF and $TiCl_4$ treatment, after annealing, and their performance in DSSCs. (a), (b) Top and lateral view, respectively; (c) J-V behavior of DSSCs with the TiO_2 NTs treated by a $TiCl_4$ solution (soaked in a 0.2 M $TiCl_4$ solution for 60 min at room temperature within airtight bottles) and various HF aqueous solution concentrations, at a constant illumination of 100 mW cm^{-2}. The dashed lines marked by k_{SH} and k_S indicate the slopes near J_{SC} and V_{OC}, respectively.

series resistance and shunt resistance, respectively.[33] Therefore the information about the electron transport in the cell can also

and compact TiO_2 NTs. By using those techniques together with the chemical treatment, the negative influence of the secondary structures might be reduced so that the efficiency can be further improved.

To ensure better identity of this study, all the following experiments were carried out preliminarily with the HF concentration at 0.35% according to previous experiments. The typical morphology of so-fabricated sample can be demonstrated by Fig. 5(a) and (b), revealing significant change with controlled modulated voltage and higher stirring rate compared to those tubes fabricated with only controlled chemical treatment. It can be clearly observed the secondary structures on the walls are more homogeneously distributed in a more uniform size. Besides, the tubes were very straight and ordered. The tubes were anodized with periodically modulated voltage of 180 ± 5 V and at stirring rate of 100 rpm and 600 rpm, which are the typical optimized values according to previous investigations.[25] Fig. 5(c) compares the J-V characteristics of the DSSCs fabricated under various conditions. The highest efficiency was 4.35% ($V_{OC} = 0.61$ V, $J_{SC} = 14.79$ mA cm^{-2}, and FF = 0.48), about 114.2% higher than the DSSC without any treatment and 19.2% higher than the sample with only chemical treatment. This result was obtained with the previously optimized chemical treatment at 180 ± 5 V with a stirring rate of 100 rpm. k_S under this condition was 2.4×10^{-2} Ω^{-1} cm^{-2}, higher than the value 2.0×10^{-2} Ω^{-1} cm^{-2} under the optimized conditions with only $TiCl_4$ and HF treatment. The k_{SH} was 1.5×10^{-3} Ω^{-1} cm^{-2}, much lower than 4.0×10^{-3} Ω^{-1} cm^{-2} for the optimized sample with $TiCl_4$ and HF. Consequently, though the short circuit current was lower than the sample when only treated by HF and $TiCl_4$, the fill factor was raised by 29.7%, which implies that the electron transport ability was further improved by better organized arrays and the real output with a certain load is much better under the same J_{SC}.

Evidently, using external modulated conditions during the anodization leads to a significant increase of the short circuit current due to both the higher surface available for dye chemisorption and the shorter path available for charge transportation. Table 1 has made a short summary of the cell performance under different conditions. In all modulated condition cases, samples fabricated by modulated voltage have a much higher short circuit current and efficiency than the samples by constant voltage, although their open circuit voltage and fill factor are slightly sacrificed. These results demonstrate that ordered and straight tubes fabricated under modulated anodic voltage are effective in increasing the performance of DSSCs based on TiO_2 NTs. In combination with the application of the other techniques which can increase the open circuit voltage, for example, improved redox pair other than the I^-/I^{3-},[35] a much better performed DSSC could be realized.

3.4.3 Mechanism of the secondary structure development. Though morphological and structural studies have indicated significant changes in those different procedures, the mechanism behind the phenomena remains unknown, *e.g.*, the reason that the formation of the secondary structures mainly happened after annealing while the sample was already taken out of the HF solution. Hence, each link of the process of the fluorination reaction and crystallization was further detected by an EDX study. It shows more information of changes that took place under different conditions. The EDX spectrum of the TiO_2 NTs without HF treatment, as shown in Fig. 6(a), indicates that the obtained nanotubes are composed of only Ti and O elements. Fig. 6(b) describes the EDX spectrum of the same TiO_2 NTs which have been sintered into crystalline films of the anatase phase. Obviously, the annealed TiO_2 NTs maintain the same elemental composition. After the fluorination reaction in HF aqueous solution, successful incorporation of elemental F into the TiO_2 nanotubes could be observed from the compositional information of the EDX spectrum in Fig. 6(c). Further annealing treatment will yield pure TiO_2 nanotubes once again, which is unambiguously illustrated by Fig. 6(d). There were only Ti and O elements left in the tube arrays, without significant existence of elemental F.

The experimental facts indicated that the formation of the secondary structures is strongly connected to the F^- anions and the high temperature annealing that followed the HF treatment. It is known that the existence of an F^- anion will induce dissolvent of TiO_2. Since the F^- is not detected after the annealing process with only TiO_2 left, the general reaction would be reversible, which is also supported by, ref. 36 with its form given as below:

Table 1 Short summary of photovoltaic characteristics of the DSSCs under various conditions [a]

	Growth and chemical treatment conditions	J_{SC}/mA cm^{-2}	V_{OC}/V	FF(%)	η(%)
Plain cell	CV [b]	6.90	0.60	49.3	2.03
HF treatment	CV, 0.1% HF	9.50	0.61	38.6	2.24
	CV, 0.2% HF	9.88	0.68	37.3	2.50
	CV, 0.35% HF	9.16	0.62	48.8	2.75
	CV, 0.5% HF	6.89	0.63	42.8	1.87
$TiCl_4$ treatment	CV, $TiCl_4$	10.09	0.62	43.8	2.76
	CV, 0.1% HF, $TiCl_4$	11.71	0.65	40.6	3.08
	CV, 0.2% HF, $TiCl_4$	13.72	0.64	39.6	3.49
	CV, 0.35% HF, $TiCl_4$	15.54	0.63	37.0	3.65
	CV, 0.5% HF, $TiCl_4$	12.27	0.64	42.6	3.36
Modulated conditions	CV, 0.35% HF, 600 rpm	11.03	0.58	54.4	3.45
	MV, [c] 0.35% HF, 100 rpm	14.23	0.56	46.9	3.75
	MV, 0.35% HF, 600 rpm	12.65	0.59	47.3	3.54
	MV, 0.35% HF, 100 rpm, $TiCl_4$	14.79	0.61	48.4	4.35

[a] All data were acquired in back-side illuminated DSSCs. [b] Constant voltage. [c] Modulated voltage.

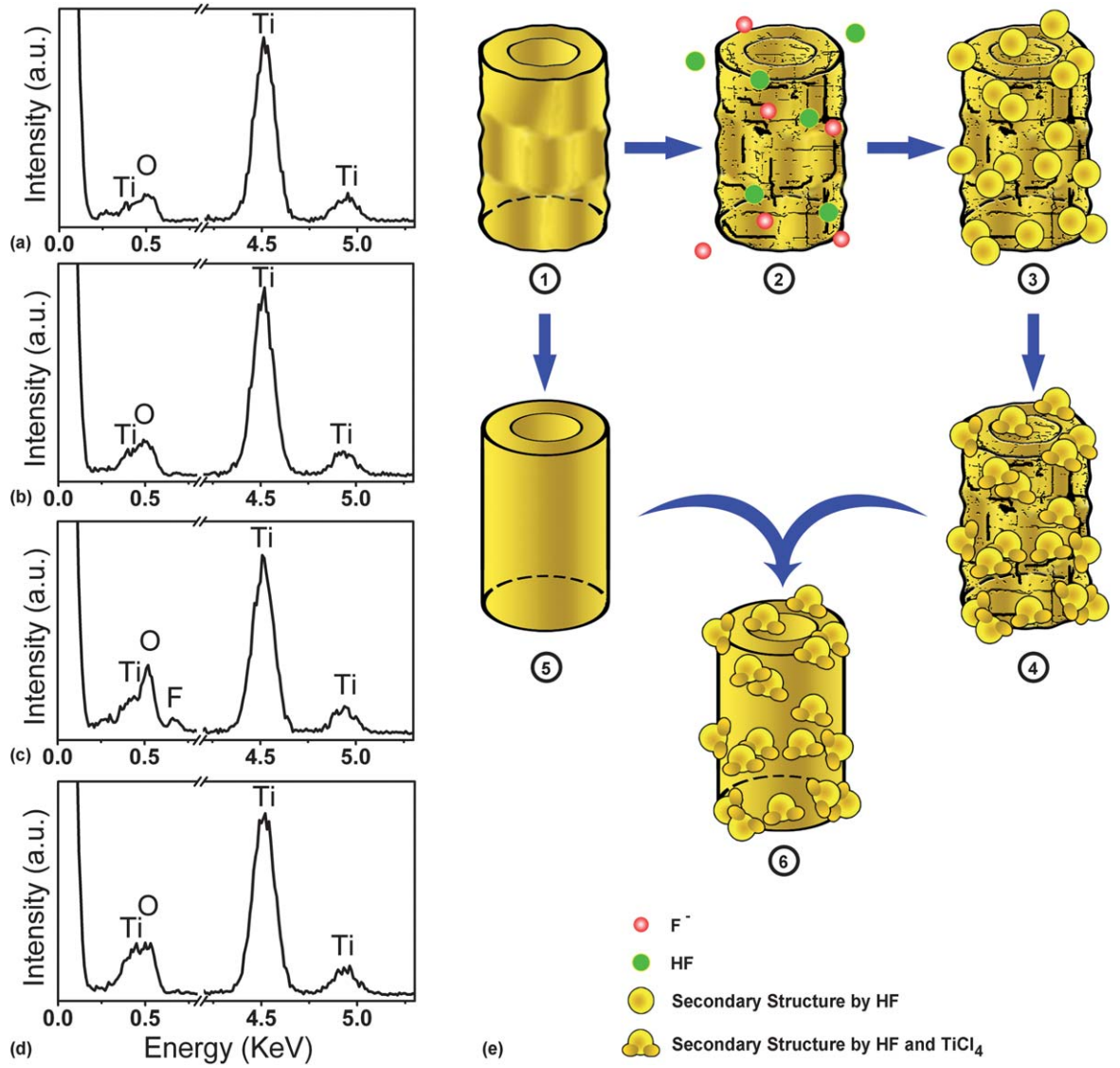

Fig. 6 Caption EDX spectroscopy of the anodized TiO_2 NTs, showing the elemental composition under different conditions. (a), (b) Without HF treatment, before and after annealing, respectively; (c), (d) with HF treatment, before and after annealing, respectively. (e) Schematic illustration, different steps of the tube modification.

$$TiO_2(s) + 4HF + 2F^- \leftrightarrow TiF_6^{2-} + 2H_2O \quad (1)$$

During the HF treatment, F components in the form of HF and F^- can diffuse into the TiO_2 bulk in different depths. However, the dissolution of TiO_2 is slow at room temperature and therefore no significant morphology change took place after the HF treatment. In the high temperature annealing, it took a certain time until the temperature finally reached the set value. During the temperature rising, more F^- in the bulk would react with the TiO_2 and induce the destruction of the TiO_2 locally. Due to the different penetrating depth, the interface between fluoride (TiF_6^{2-}) and TiO_2 becomes much rougher, as shown in the step (2) in Fig. 6(e). As a consequence, there would be a redistribution of fluoride due to the rough TiO_2 surface and diffusion under high temperature. Nevertheless, as the temperature continues to rise up and being kept at several hundred degrees, the fluoride turns into TiO_2 again, and forms particle like secondary structures, as shown in the step (3) in Fig. 6(e). Starting from a tiny value, if the $[F^-]$ is gradually increased with increasing HF concentration, this reformation will be enhanced, so that more secondary structures will develop. However, if $[F^-]$ becomes too high, then TiO_2 dissolvent would be significantly enhanced even at room temperature, which could be the reason for the smooth and thin tubes formed with 0.5% HF shown in Fig. 3(d).

When $TiCl_4$ was applied on the HF treated and annealed sample, a part of the Ti^{4+} ions will be enriched near the contact of secondary structures and the TiO_2 tubes. After the second annealing, new minor TiO_2 crystals will be formed near those positions, as shown in the step (4) in Fig. 6(e). Therefore they could further increase the effective contact surface area and enhance the ability of electron transport from the surface to the bulk. However, these minor contacts can not repair the damage inside the tube bulks. According to common comprehensions on corrosion processes, the chemical etching can be excessively

enhanced in certain positions with stronger roughness (step (1) in Fig. 6(e)).[37] Therefore the electron transport of the originally rough tubes before the chemical treatment will suffer more from the structural damaging compared to the originally smooth and straight ones. Besides, it is easier for the $TiCl_4$ treatment to form unnecessary contacts on the originally roughened surface than on the smooth and ordered tubes, which increases the probability of carrier recombination, leading to lower shunt resistance and fill factor.

Fortunately, as introduced in sec. 3.4.2, straight and ordered tubes could be formed in a high growth rate with controlled mechanical stirring and periodically modulated voltages (step (5) in Fig. 6(e)).[25] With those tubes, the damage in the bulk by the chemical treatment can be relatively reduced. Additionally, straighter, ordered tubes also helps to reduce the blocking effect from enhanced roughness inside the tubes after the chemical treatment. Consequently, the efficiency of DSSCs based on so-fabricated tube arrays was further improved. The composite structures were shown in the step (6) in Fig. 6(e) and the photovoltaic characteristics were summarized in Table 1. It is interesting to observe that a large amplification of 114% has been achieved by all of above treatments compared to the plain sample without any treatment.

4. Conclusions

To summarize this work, it can be concluded that a suitable balance can be generally established among the paradox in the dye absorption, the electron transportation at the surface and the bulk. First, the secondary structures can be controllably grown on both sides of the TiO_2 tubes developed with HF treatment, which induces a significant increase (>35%) of the conversion efficiency in DSSCs. With a subsequent $TiCl_4$ treatment and application of controlled oscillatory conditions, the negative effect to the electron transport in the cell due to the chemical treatments can be reduced. Overall, an efficiency of 4.35% can be reached in the back-side illuminated DSSC, which is ~114% higher than the basic value. Based on that, greater efficiency improvements of nanotube based DSSCs with thin layer thickness could be hopefully realized, with the development of other key parts, such as new dyes and electrolytes based on a new redox pair.[5,35,38,39]

Acknowledgements

This work was supported by the National Major Basic Research Project of 2012CB934302, Natural Science Foundation of China under contracts 11074169 and 11174202.

Notes and references

1 O. K. Varghese, D. Gong, M. Paulose, K. G. Ong and C. A. Grimes, *Sens. Actuators, B*, 2003, **93**, 338.
2 H. Tsuchiya, J. M. Macak, L. Müller, J. Kunze, F. Müller, P. Greil, S. Virtanen and P. Schmuki, *J. Biomed. Mater. Res., Part A*, 2006, **77**, 534.
3 J. M. Macak, M. Zlamal, J. Krysa and P. Schmuki, *Small*, 2007, **3**, 300.
4 B. O'Regan and M. Grätzel, *Nature*, 1991, **353**, 737.
5 A. Yella, H. W. Lee, H. N. Tsao, C. Yi, A. K. Chandiran, M. K. Nazeeruddin, E. W. G. Diau, C. Y. Yeh, S. M. Zakeeruddin and M. Grätzel, *Science*, 2011, **334**, 629.
6 T. Y. Peng, A. Hasegawa, J. R. Qiu and K. Hirao, *Chem. Mater.*, 2003, **15**, 2011.
7 M. Law, L. E. Greene, J. C. Johnson, R. Saykally and P. D. Yang, *Nat. Mater.*, 2005, **4**, 455.
8 K. Zhu, N. R. Neale, A. Miedaner and A. J. Frank, *Nano Lett.*, 2007, **7**, 69.
9 J. R. Jennings, A. Ghicov, L. M. Peter, P. Schmuki and A. B. Walker, *J. Am. Chem. Soc.*, 2008, **130**, 13364.
10 P. Roy, D. Kim, K. Lee, E. Spiecker and P. Schmuki, *Nanoscale*, 2010, **2**, 45.
11 S. Agarwala, M. Kevin, A. S. Wong, C. K. Peh, V. Thavasi and G. W. Ho, *ACS Appl. Mater. Interfaces*, 2010, **2**, 1844.
12 J. M. Macak, H. Tsuchiya, A. Ghicov and P. Schmuki, *Electrochem. Commun.*, 2005, **7**, 1133.
13 D. Kim, A. Ghicov, S. P. Albu and P. Schmuki, *J. Am. Chem. Soc.*, 2008, **130**, 16454.
14 D. Kuang, J. Brillet, P. Chen, M. Takata, S. Uchida, H. Miura, K. Sumioka, S. M. Zakeeruddin and M. Grätzel, *ACS Nano*, 2008, **2**, 1113.
15 P. Charoensirithavorn, Y. Ogomi, T. Sagawa, S. Hayase and S. Yoshikawa, *J. Electrochem. Soc.*, 2010, **157**, B354.
16 F. Sauvage, F. Di Fonzo, A. Li Bassi, C. S. Casari, V. Russo, G. Divitini, C. Ducati, C. E. Bottani, P. Comte and M. Graetzel, *Nano Lett.*, 2010, **10**, 2562.
17 O. K. Varghese, M. Paulose, K. Shankar, G. K. Mor and C. A. Grimes, *J. Nanosci. Nanotechnol.*, 2005, **5**, 1158.
18 C. A. Grimes, G. K. Mor, K. Shankar, M. Paulose and O. K. Varghese, *Nano Lett.*, 2006, **6**, 215.
19 C. Richter and C. A. Schmuttenmaer, *Nat. Nanotechnol.*, 2010, **5**, 769.
20 J. Wang and Z. Q. Lin, *Chem. Mater.*, 2010, **22**, 579.
21 S. Ito, P. Liska, P. Comte, R. L. Charvet, P. Pechy, U. Bach, L. Schmidt-Mende, S. M. Zakeeruddin, A. Kay, M. K. Nazeeruddin and M. Grätzel, *Chem. Commun.*, 2005, 4351.
22 B. C. O'Regan, J. R. Durrant, P. M. Sommeling and N. J. Bakker, *J. Phys. Chem. C*, 2007, **111**, 14001.
23 L. M. Peter, *Phys. Chem. Chem. Phys.*, 2007, **9**, 2630.
24 C. He, Z. Zheng, H. L. Tang, L. N. Zhao and F. Lu, *J. Phys. Chem. C*, 2009, **113**, 10322.
25 H. Liu, L. Tao and W. Z. Shen, *Nanotechnology*, 2011, **22**, 155603.
26 H. Liu, L. Tao and W. Z. Shen, *Electrochim. Acta*, 2011, **56**, 3905.
27 Q. Q. Hou, Y. Z. Zheng, J. F. Chen, W. L. Zhou, J. Deng and X. Tao, *J. Mater. Chem.*, 2011, **21**, 3877.
28 T. Ohsaka, F. Izumi and Y. Fujiki, *J. Raman Spectrosc.*, 1978, **7**, 321.
29 W. F. Zhang, Y. L. He, M. S. Zhang, Z. Yin and Q. Chen, *J. Phys. D: Appl. Phys.*, 2000, **33**, 912.
30 A. S. Pottier, S. Cassaignon, C. Chaneac, F. Villain, E. Tronc and J. P. Jolivet, *J. Mater. Chem.*, 2003, **13**, 877.
31 A. J. Frank, N. Kopidakis and J. van de Lagemaat, *Coord. Chem. Rev.*, 2004, **248**, 1165.
32 K. Zhu, T. B. Vinzant, N. R. Neale and A. J. Frank, *Nano Lett.*, 2007, **7**, 3739.
33 C. Y. Chang and F. Y. Tsai, *J. Mater. Chem.*, 2011, **21**, 5710.
34 S. Ito, T. N. Murakami, P. Comte, P. Liska, C. Gratzel, M. K. Nazeeruddin and M. Grätzel, *Thin Solid Films*, 2008, **516**, 4613.
35 M. Wang, N. Chamberland, L. Breau, J. E. Moser, R. Humphry-Baker, B. Marsan, S. M. Zakeeruddin and M. Grätzel, *Nat. Chem.*, 2010, **2**, 385.
36 D. Gutiérrez-Tauste, X. Domènech, N. Casañ-Pastor and J. A. Ayllón, *J. Photochem. Photobiol., A*, 2007, **187**, 45.
37 L. R. Hilbert, D. Bagge-Ravn, J. Kold and L. Gram, *Int. Biodeterior. Biodegrad.*, 2003, **52**, 175.
38 D. Li, H. Li, Y. Luo, K. Li, Q. Meng, M. Armand and L. Chen, *Adv. Funct. Mater.*, 2010, **20**, 3358.
39 T. Daeneke, T. H. Kwon, A. B. Holmes, N. W. Duffy, U. Bach and L. Spiccia, *Nat. Chem.*, 2011, **3**, 211.

